Coral Reefs (2015) 34:215–229
DOI 10.1007/s00338-014-1234-2

REPORT

Sediment accumulation, stratigraphic order, and the extent of time-averaging in lagoonal sediments: a comparison of ^{210}Pb and ^{14}C/amino acid racemization chronologies

Matthew A. Kosnik · Quan Hua · Darrell S. Kaufman · Atun Zawadzki

Received: 26 July 2014 / Accepted: 13 October 2014 / Published online: 15 November 2014
© The Author(s) 2014. This article is published with open access at Springerlink.com

Abstract Carbon-14 calibrated amino acid racemization (^{14}C/AAR) data and lead-210 (^{210}Pb) data are used to examine sediment accumulation rates, stratigraphic order, and the extent of time-averaging in sediments collected from the One Tree Reef lagoon (southern Great Barrier Reef, Australia). The top meter of lagoonal sediment preserves a stratigraphically ordered deposit spanning the last 600 yrs. Despite different assumptions, the ^{210}Pb and ^{14}C/AAR chronologies are remarkably similar indicating consistency in sedimentary processes across sediment grain sizes spanning more than three orders of magnitude (0.1–10 mm). Estimates of long-term sediment accumulation rates range from 2.2 to 1.2 mm yr^{-1}. Molluscan time-averaging in the taphonomically active zone is 19 yrs, whereas below the depth of final burial (~15 cm), it is ~110 yrs/5 cm layer. While not a high-resolution paleontological record, this reef lagoon sediment is suitable for paleoecological studies spanning the period of Western colonization and development. This sedimentary deposit, and others like it, should be useful, albeit not ideal, for quantifying anthropogenic impacts on coral reef systems.

Keywords Carbonate sediment · Late Holocene · One Tree Reef lagoon · Bivaliva · *Abranda jeanae*

Communicated by Handling Editor Chris Perry

Electronic supplementary material The online version of this article (doi:10.1007/s00338-014-1234-2) contains supplementary material, which is available to authorized users.

M. A. Kosnik (✉)
Department of Biological Sciences, Macquarie University, Macquarie University, NSW 2109, Australia
e-mail: mkosnik@alumni.uchicago.edu

Q. Hua · A. Zawadzki
Australian Nuclear Science and Technology Organisation, Locked Bag 2001, Kirrawee DC, NSW 2232, Australia
e-mail: qhx@ansto.gov.au

A. Zawadzki
e-mail: aab@ansto.gov.au

D. S. Kaufman
School of Earth Sciences and Environmental Sustainability, Northern Arizona University, Flagstaff, AZ 86011-4099, USA
e-mail: Darrell.Kaufman@nau.edu

Introduction

Determining the chronological framework of sedimentary deposits is paramount for studying past and modern sedimentary systems. Carbonate sedimentary deposits are diverse assemblages of skeletal fragments that are mixed and altered by a variety of physical and biological processes. The combination of varied origins and taphonomic histories makes understanding reef-associated sedimentary deposits especially challenging. The desire to use reef sediment deposits to quantify anthropogenic impacts over the last few hundred yrs provides clear criteria against which to evaluate the temporal resolution of these fossil records.

Chronology in sedimentary systems comprises two key parameters. The most commonly quantified parameter is the relation between age and burial depth within the sediment. While this parameter is critical, it is a single value, and the variation around this value is rarely quantified beyond the analytical uncertainty of the dating method. The second key parameter, time-averaging, is the amount of time represented in a sedimentary deposit, or stratigraphic unit (Flessa et al. 1993; Kowalewski 1996). While the mean age of a sedimentary assemblage is important, it is the age distribution of the constituents within the

sedimentary sample, or time-averaging, which fundamentally limits the temporal resolution of a given deposit. Quantifying time-averaging is time- and resource-intensive, so although it is of utmost importance for understanding the processes underlying nearly all paleontological and sedimentological investigations, few studies date a sufficient number of specimens to quantify the age distribution.

Lack of quantitative estimates of time-averaging was not a problem when paleontologists thought about temporal resolution at a coarse scale. Now, however, paleoecological studies spanning the period of colonial expansion and/or anthropogenic impact require a detailed understanding of the formation of the fossil assemblages being utilized. Although time-averaging in tropical sedimentary deposits is still comparatively understudied (see Kidwell et al. 2005; Krause et al. 2010; Kosnik et al. 2013), previous work has shown that reefal sediment accumulating over the past few hundred yrs is not necessarily stratigraphically ordered (Kosnik et al. 2007, 2009, 2013). One needs look no further than volume 11 issue 2 of *Coral Reefs* to see the controversy caused by the use of paleontological data derived from reefal sediment to examine the Holocene history of Crown-of-thorns outbreaks on the Great Barrier Reef (GBR). The most detailed critiques can be found in Fabricius and Fabricius (1992), Keesing et al. (1992), and Pandolfi (1992), but the key criticisms of the Walbran et al. (1989) study were the effect of post-death processes on the preservation of the spicules (i.e., taphonomy) and the methods used to estimate the age of the samples (i.e., chronology).

A number of factors determine the temporal resolution of a fossil assemblage. First, the sedimentation rate determines the minimum possible degree of time-averaging, with higher rates of sedimentation typically resulting in less time-averaging (Meldahl et al. 1997). Second, the rate and depth of mixing, either physical or biogenic, determine the maximum possible degree of time-averaging, with deeper and faster sediment mixing leading to more time-averaging (Olszewski 2004). Some bioturbators active in tropical sediments (e.g., callianassid shrimp) can effectively sort sedimentary grains by size, shape, and/or other characteristics (Tudhope and Scoffin 1984). Third, sediment grain durability determines the length of time that a sedimentary particle will remain intact and recognizable. Fragile sedimentary particles are more likely to be destroyed (e.g., fragmented, eroded, or dissolved) during mixing, leading to less time-averaging, whereas durable particles can be thoroughly mixed without breaking, leading to more time-averaging (Cummins et al. 1986; Kosnik et al. 2009).

Here, we examine the sediment accumulating in the One Tree Reef (OTR) lagoon to determine the suitability of this lagoonal sediment for paleoecological analyses on the timescales associated with European colonization and the economic development of the Australian continent. We use two independent methods to establish chronologies: 1. Lead-210 (^{210}Pb) is a naturally occurring isotope associated with fine-grained sediments. It is commonly used to determine the age of sediments less than $\sim$150 yrs. 2. Carbon-14 calibrated Amino Acid Racemization (^{14}C/AAR) directly dates individual mineralized skeletal elements, and it is commonly used to determine the age of Holocene molluscan shells. These two methods have entirely distinct assumptions and potential biases, so they are well suited for cross-validation.

Materials and methods

Study site

One Tree Reef (OTR) is an outermost reef in the Capricorn group at the southern end of the GBR, Australia (Fig. 1). The OTR lagoon is entirely rimmed by reef crest and isolated from the ocean at large for much of the tidal cycle (the lagoon ponds at $\sim$1.5 m above lowest astronomical tide). The main lagoon is shallow, reaching a maximum ponded depth of approximately 6 m near the northern edge, and it contains many small patch reefs that reach the ponded surface. At the shallow southern and eastern edges, the lagoonal sediment is dominated by coarse sand, while at the deeper northern edge the sediment is dominantly fine mud. OTR has been comparatively well studied due to the presence of the One Tree Island Research Station operated by the University of Sydney.

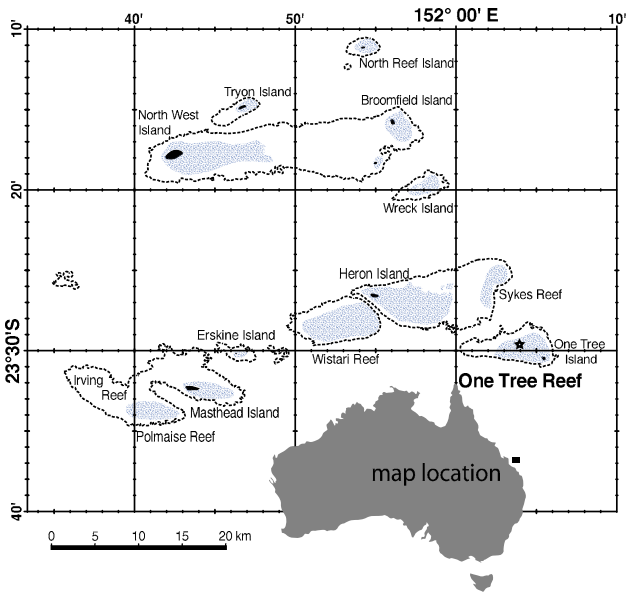

Fig. 1 Map of the Capricorn reefs, southern Great Barrier Reef, Australia (derived from Great Barrier Reef Marine Park Authority zoning map 18, 2011)

Relative to many shallow tropical lagoons, the OTR lagoon contains very fine sediments and very low callianassid shrimp activity. Very few places in the OTR lagoon have anything approaching the classic "callianassid volcano-field" topography observed in many coral reef lagoons. No site in the main lagoon showed signs of anything more than minor burrowing activity throughout field activities in 2012 and 2013 (Kosnik pers. obs.). The area sampled for this study had a flat surface with only a low density of small burrow holes indicating the presence of a bioturbating fauna.

In September 2012, sediments from the northwestern end of the main OTR lagoon were collected using 80 mm hand cores and a 0.5 m × 0.5 m excavation. The ponded water depth at the collection site (23.49677°S, 152.06587°E) was 4.5 m. Here, we focus on a single 1.6 m deep 80 mm diameter percussive hand core and a single 1.2 m deep 0.25 m^2 excavation both collected by divers. The method of excavation differs slightly from previous work at Rib and Bramble Reefs (Kosnik et al. 2007, 2009, 2013) in that the retaining wall system was assembled without mechanized assistance and the layers were collected using an 80 mm diameter water dredge rather than an 80 mm diameter airlift. The water dredge was fitted with a small water jet to facilitate the gentle breakup of the compacted mud. As in previous studies, the excavation was collected in 5 cm layers into ~1 mm mesh bags, so complete grain size analysis of the excavated sample was not possible. The most abundant bivalve, *Abranda jeanae*, was selected as a representative mollusk from the >4 mm sieve size fraction for dating analyses (Fig. 2). Hand cores were taken ~0.2 m away from the excavation site in order to examine the full grain size distribution and to sample the fine sediment fraction required for ^{210}Pb dating.

The depth of each excavation layer was measured relative to a fixed datum and is expressed as excavation depth. The 5 cm collection layers determine the finest possible depth resolution of the ^{14}C/AAR dataset. The hand core was split and sampled in 1 cm thick layers. The penetration and recovery of the hand core were measured during collection, but before processing the hand core compressed 2 cm. There are a variety of quantitative methods for uncompressing the core and returning these 2 cm to the total core length, but since the primary goal of this study is to compare the two chronologies and both the original and compressed hand core depths correlate with the same excavation layer, we use compressed core depths which are 2 cm less than the collected core depths.

Sediment description

The hand core was visually homogeneous with no indication of layering or change in sediment characteristics down core. The hand core was subsampled for grain size analyses every 5 cm (i.e., 0–1, 5–6, 10–11, 15–16 cm, etc.) to align with the 5 cm thick excavation layers. These sediment samples were suspended in 15 ml of dispersant and 15 ml of distilled water by spinning for an hour before being injected into a Malvern Mastersizer 2000 where an average of three measurements was used to determine the grain size distribution. We use the 10th, 50th, and 90th quantile grain sizes provided by the Mastersizer software to characterize the grain size distribution through the ~1.6 m core length.

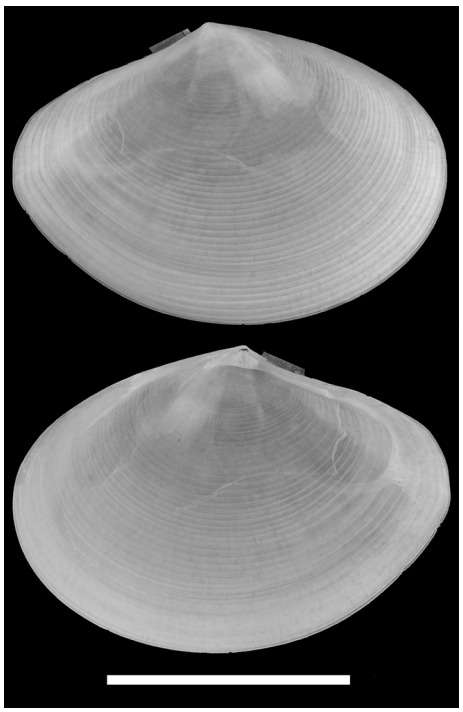

Fig. 2 A right valve of *Abranda jeanae*. The *scale bar* is 10 mm. The photographed specimen is deposited at the Australian Museum, Sydney (C.478298)

^{210}Pb age determination

Bulk sediment samples from the hand core were dated at the Australian Nuclear Science and Technology Organisation (ANSTO) Environmental Radioactivity Measurement Centre using the ^{210}Pb method, which has been used over the past 4 decades to date recent aquatic sediments up to 150 yrs old (Goldberg 1963; Appleby and Oldfield 1978; Oldfield and Appleby 1984; Appleby 2001). Dating is based upon the determination of the vertical distribution of unsupported ^{210}Pb, a naturally occurring radionuclide that is present in aquatic sediment as a result of atmospheric fallout. By taking samples at regular intervals over the length of a sediment core and determining the atmospherically derived ^{210}Pb activity, a chronology can be established, and a sedimentation rate calculated. The total ^{210}Pb

activity in sediments has two components: supported ^{210}Pb activity ($^{210}Pb_s$) derived from the decay of in situ radium-226 (^{226}Ra), and unsupported ^{210}Pb activity ($^{210}Pb_u$) derived from atmospheric fallout. $^{210}Pb_s$ activity can be determined indirectly via its grandparent radioisotope ^{226}Ra. $^{210}Pb_u$ activity is estimated by subtracting $^{210}Pb_s$ activity from the total activity of ^{210}Pb ($^{210}Pb_t$) or its progeny polonium-210 (^{210}Po) (Hollins et al. 2011).

To measure ^{210}Po and ^{226}Ra activities, approximately 5 g of dried sediment was spiked with artificial ^{209}Po and ^{133}Ba tracers. Each sediment sample was subsequently leached with hot concentrated acids to release polonium and radium. Polonium was auto-plated onto silver disks after adding the reducing agent hydroxylammonium chloride. Radium was co-precipitated with $BaSO_4$ and collected on a fine-resolution filter paper. Each polonium disk and radium filter sources were counted by high-resolution alpha spectrometry. The activity of the artificial tracer ^{209}Po on the polonium disk, determined by alpha spectrometry, was used to calculate the ^{210}Po chemical recovery. The chemical recovery for ^{226}Ra was determined by measuring the artificial tracer ^{133}Ba on a High Purity Germanium (HPGe) gamma detector. The $^{210}Pb_u$ activity for each sample was calculated, and the sediment core chronology was determined using the constant initial concentration (CIC) and constant rate of supply (CRS) ^{210}Pb age models (Appleby 2001).

The CIC age model was fit using the six samples (between 0.15 and 0.41 m), excluding the three samples (between 0 and 0.11 m) at the top of the core and the two deepest layers where $^{210}Pb_u$ activities were not different than zero. CIC ages were estimated for the upper three layers by linear extrapolation. The CRS age model was fit using all nine samples analyzed where $^{210}Pb_u$ activities were greater than zero (0–0.41 m). Of note, the CRS age estimate for the 0.40–0.41 m layer has extremely high uncertainty due to the very low $^{210}Pb_u$ activity measured. All of the ^{210}Pb-derived ages are relative to the year of collection (2012 AD), and the data are summarized in Table 1.

Abranda jeanae

The most abundant mollusk sampled in the excavation layers and in the living assemblage, *Tellina (Abranda) jeanae* Healy and Lamprell 1992 (Bivalvia: Tellinidae: Tellininae), is relatively large and thin shelled (Fig. 2). The figured specimen has been deposited in the Malacology Collection at the Australian Museum, Sydney (C.478298). Only complete right valves in good condition were analyzed to exclude the possibility of analyzing the same individual twice. The posterior halves of 80 disarticulated right valves were used for AAR analyses. Based on AAR results, the anterior halves of eleven shells were used for AMS ^{14}C dating. The geometric mean size of dated specimens ranged from 4.9 to 10.8 mm with a median size of 8.4 mm. There was no correlation between dated specimen size and excavation depth ($p = 0.64$).

Amino acid racemization

Single samples from 80 *Abranda* right valves were prepared for amino acid analysis at Northern Arizona University according to standard procedure (Wehmiller and Miller 2000). The shells were cleaned by acid leaching, then each fragment was weighed and demineralized in 20 ml of 7 M HCl mg^{-1} of $CaCO_3$. The total hydrolyzable amino acid (THAA) population of amino acids was recovered by hydrolyzing the sample solutions under N_2 at 110 °C for 6 h. This hydrolysis procedure minimizes the amount of induced racemization in the most rapidly racemizing amino acids, especially for young shells, while the recovery of amino acids is near maximum (Kaufman and Manley 1998). Sample solutions were evaporated to dryness in vacuo and then rehydrated in 0.01 M HCl containing an internal standard of L-homo-arginine of known concentration for calculating the concentration of amino acids relative to the mass of shell. Each sample was analyzed once using reverse-phase, high-performance liquid chromatography (HPLC). All chromatograms were of consistently high quality, and none was rejected.

The chromatographic instrumentation and procedure used to separate amino acid enantiomers was described by Kaufman and Manley (1998). Briefly, the analytical method employed pre-column derivatization with o-phthaldialdehyde together with the chiral thiol, *N*-isobutyryl-L-cysteine, to yield fluorescent diastereomeric derivatives of chiral (D and L) amino acids. The derivatization was performed online prior to each injection using the auto-injector of an integrated Agilent 1100 HPLC. Separation was by a reverse-phase column packed with a C_{18} stationary phase (Hypersil BDS, 5 mm) using a linear gradient of aqueous sodium acetate, methanol, and acetonitrile. Detection was by fluorescence.

We focused on eight amino acids: aspartic acid (Asp), glutamic acid (Glu), serine (Ser), alanine (Ala), valine (Val), phenylalanine (Phe), alloisoleucine/isoleucine (A/I), and leucine (Leu) that are abundant in molluscan-shell protein, and resolvable by reverse-phase HPLC. The Asp and Glu values may include a small component of asparagine and glutamine, respectively, which were converted to Asp and Glu during laboratory hydrolysis. D/L values for all eight amino acids are reported in the Electronic Supplementary Material (ESM 1).

Table 1 Hand core and lead-210 data used to determine the relation between sediment age and depth

ANSTO ID	Sediment			^{210}Pb activity (Bq/kg)		Modelled age (yr) (compressed)		Modelled age (yr) (collected depth)	
	Depth (m)	Density (g cm^{-3})	Cumulative mass (g)	Total	Unsupported	CIC	CRS	CIC	CRS
P168	0.00–0.01	1.5	3.7 ± 0.7	8.7 ± 0.4	6.0 ± 0.4	1 ± 1	1 ± 1	7 ± 2	3 ± 2
P169	0.05–0.06	1.3	10.7 ± 0.7	10.2 ± 0.4	7.9 ± 0.4	14 ± 2	7 ± 3	20 ± 3	9 ± 3
P170	0.10–0.11	1.4	17.6 ± 0.7	8.4 ± 0.4	6.8 ± 0.4	27 ± 4	16 ± 4	32 ± 4	18 ± 4
P359	0.15–0.16	1.5	24.8 ± 0.7	9.3 ± 0.4	7.7 ± 0.4	40 ± 5	28 ± 5	46 ± 6	30 ± 5
P171	0.20–0.21	1.5	32.2 ± 0.7	6.7 ± 0.3	4.5 ± 0.3	54 ± 7	43 ± 7	59 ± 8	45 ± 7
P360	0.25–0.26	1.4	39.5 ± 0.7	6.0 ± 0.3	4.1 ± 0.3	67 ± 9	61 ± 8	73 ± 9	63 ± 4
P172	0.30–0.31	1.4	46.5 ± 0.7	3.6 ± 0.2	2.5 ± 0.2	80 ± 10	86 ± 9	86 ± 11	88 ± 7
P361	0.35–0.36	1.3	53.2 ± 0.7	3.1 ± 0.2	1.1 ± 0.2	92 ± 12	116 ± 11	98 ± 12	118 ± 11
P173	0.40–0.41	1.4	59.8 ± 0.7	2.6 ± 0.1	1.1 ± 0.2	104 ± 13	257 ± 104	110 ± 14	259 ± 104
P362-1	0.50–0.51	1.3	73.0 ± 0.7	1.5 ± 0.1	0.1 ± 0.2				
P362-2	0.50–0.51		73.0 ± 0.7	1.5 ± 0.1					
P363-1	0.54–0.55	1.2	78.6 ± 0.7	1.6 ± 0.1	0.4 ± 0.2				
P363-2	0.54–0.55		78.6 ± 0.7	2.0 ± 0.1					

Sediment depth (meters), density (g cm^{-3}), and cumulative mass (g) refer to the sediment core after post-collection compaction. Sediment constant initial concentration (CIC) and constant rate of supply (CRS) models are used to determine the age (yrs before collection) of each layer

Radiocarbon dating

From the 80 *Abranda* analyzed for AAR, eleven shells spanning the range of observed D/L values were selected for AMS ^{14}C dating using the suite of criteria outlined in Kosnik and Kaufman (2008) and Kosnik et al. (2008). Prior to AMS analysis, shell fragments were physically cleaned and ~30 % of the remaining mass was removed with 0.125 M HCl. Pretreated samples were hydrolyzed to CO_2 using 85 % H_3PO_4, then converted to graphite using the Fe/H_2 method (Hua et al. 2001). AMS ^{14}C measurements were taken at ANSTO using the STAR facility (Fink et al. 2004). Radiocarbon ages were converted to calendar years using OxCal 4.1 program (Bronk Ramsey 2009), Marine09 data (Reimer et al. 2009), and a regional marine reservoir correction (ΔR) value of 4 ± 40 yrs based on the mean ^{14}C offset between the Marine09 curve and the known-age coral core from Abraham Reef (Druffel and Griffin 2004) for the period 1635–1950 AD. The median of the age probability function was used as the calendar age, and the 2σ age range was used as the age uncertainty. All amino acid inferred ages discussed herein are calendar years relative to 2012 AD, the year of core collection (2012 AD ≡ 0 yr, Table 2). The results are the same for any year zero (i.e., 1950 AD), but the interpretation is clearer when the shell ages are set relative to the time that they were collected. Radiocarbon ages ranged from 28 to 617 yrs before collection. The radiocarbon data are summarized in Table 2.

Abranda age determination

A single best age estimate was determined for each *Abranda* valve using AAR calibration models that were created using the Bayesian model fitting procedures outlined in and analytical scripts provided by Allen et al. (2013). In all, 72 different age models were fit using R 3.02 (R Development Core Team 2013). The lognormal distribution was the preferred uncertainty distribution because using the gamma distribution to model uncertainty led to systematic overestimates of the ages of specimens less than ~32 yrs (ESM 2). While six amino acid D/L values (Asp, Glu, Ala, Val, Phe, Leu) were fit, only Asp and Glu D/L contributed to the averaged gamma uncertainty model and only Asp D/L contributed to the averaged lognormal uncertainty model (ESM 3). Three mathematical functions were fit [time-dependent rate kinetics (TDK), constrained power-law kinetics (CPK), simple power-law kinetics (SPK)] with and without fitting a non-zero initial D/L value (R_0). Only TDK and SPK contributed to the final averaged model (Table 3). Time-dependent rate kinetics with a fit initial D/L value contributed 83 % of the averaged lognormal age model (Table 3). The Bayesian posterior distributions for the parameters of each age model are plotted in ESM 4. The shell ages used for this study are derived from Bayesian model averaging of models fit using the lognormal distribution to estimate uncertainty and only aspartic acid contributed to the final age model (Table 3).

Table 2 Absolute age data used to fit age-D/L models. The specimen number is the specimens' unique identification number, UAL ID is the unique identification number for AAR analyses at Northern Arizona University and links these data to the D/L data in ESM 1, and ANSTO ID is the unique identifier for the radiocarbon analyses at the Australian Nuclear Science and Technology Organisation

Specimen number	AAR data	Radiocarbon data									
	UAL ID	ANSTO ID	$\delta^{13}C$	Conventional (BP)		Calibrated (cal yr BP)			Calibrated (yr)		
				Age	1σ unc.	Age	2σ age range		Age	2σ age range	
16829	9763	OZP964	1.9	NA	NA	−34	−41	−20	28	21	42
16866	9774	OZP965	2.4	455	40	80	0	230	142	62	292
16865	9773	OZP966	2.4	480	30	100	0	235	162	62	297
16944	9807	OZP967	2.3	560	45	180	0	295	242	62	357
16919	9793	OZP968	2.7	710	25	355	265	455	417	327	517
16889	9779	OZP969	1.9	960	25	555	485	635	617	547	697
16922	9796	OZP970	2.6	785	30	420	305	500	482	367	562
16918	9792	OZP971	2.6	765	30	400	295	490	462	357	552
16868	9776	OZQ668	2.0	455	30	75	0	230	137	62	292
16895	9785	OZQ669	3.4	895	30	505	430	610	567	492	672
16928	9802	OZQ670	2.4	875	30	490	405	600	552	467	662
14651	8828	Live collected							1	0.1	2
14652	8835	Live collected							1	0.1	2
14653	8831	Live collected							1	0.1	2
14654	8830	Live collected							1	0.1	2
14655	8834	Live collected							1	0.1	2
14656	8829	Live collected							1	0.1	2
14657	8827	Live collected							1	0.1	2
14658	8825	Live collected							1	0.1	2
14659	8824	Live collected							1	0.1	2
14660	8826	Live collected							1	0.1	2
14661	8833	Live collected							1	0.1	2
14662	8832	Live collected							1	0.1	2

All specimens were calibrated using OxCal 4.1, the Marine09 calibration curve, and an ΔR of 4 ± 40 yrs. Calibrated age (cal yr BP) is relative to 1950 AD. Calibrated age (yrs) is relative to 2012 AD, the yr of collection

Time-averaging

Time-averaging, like any estimate of variation, is sensitive to sample size. Despite sampling sediment volumes 50 times larger than a typical hand core (each 5 cm excavation layer sampled 0.0125 vs. the 0.00025 m^3 sampled by an equivalent 5 cm layer from the hand core), the number of *Abranda* dated was fundamentally limited by the number of right valves sampled. As each 5 cm excavation layer is represented by ~10 *Abranda* valves, an estimate of time-averaging based on the two standard deviation age range (2σ or 95 % of the data as defined by 0.977–0.023 quantile range) is essentially the full range of ages recorded in the sample and thus the difference between the two most extreme ages. The one standard deviation (1σ) age range equivalent to 68 % of the data (0.841–0.159 quantile range) is essentially the average age of the 2nd and 3rd oldest shells minus the average age of the 2nd and 3rd youngest shells. Consequently, we use the quantiles associated with the 1σ age range to characterize the extent of time-averaging to minimize our reliance on the most extreme age estimates in each layer, but both the 1σ and 2σ time-averaging estimates are provided in Table 4. All quantiles were calculated using the quantile() function in R 3.02, using the default method of linear interpolation between continuous points (type 7).

Results

Sediment description

The grain size distribution was consistent throughout the entire 1.6 m length of the hand core (Fig. 3). The median grain size was 85 μm, the 10th quantile was 30 μm, and the 90th quantile was 456 μm. Sieved fractions from the excavated layers were also consistent down core with 31 % by dry weight 1–2 mm grains, 44 % 2–4 mm grains, and

Table 3 Bayesian model averaging summary by uncertainty distribution

Function	Amino acid	ln(a)	ln(b)	c	R_0	ln(d)	k	n	BIC	ΔBIC	wBIC	Model
Lognormal												
TDK1	Asp	10.393	0.996	0.332	0.008	−2.254	4	23	147.40	0.00	0.83	11
SPK0	Asp	12.128	1.400	–	≡0.000	−1.949	3	23	152.14	4.74	0.08	9
TDK0	Asp	11.993	1.389	–	≡0.000	−1.921	3	23	153.00	5.60	0.05	8
SPK1	Asp	11.619	1.320	0.908	0.010	−2.045	4	23	153.29	5.89	0.04	12
Gamma												
TDK1	Glu	10.939	0.649	0.748	0.010	2.050	4	23	176.88	0.00	0.27	17
SPK0	Glu	12.784	1.032	–	≡0.000	2.443	3	23	178.49	1.61	0.12	15
SPK1	Glu	12.046	0.912	1.349	0.012	2.129	4	23	178.49	1.61	0.12	18
TDK0	Glu	12.758	1.030	–	≡0.000	2.428	3	23	178.54	1.66	0.12	14
SPK0	Asp	10.318	1.068	–	≡0.000	2.401	3	23	178.56	1.67	0.11	3
TDK0	Asp	10.177	1.047	–	≡0.000	2.420	3	23	178.84	1.96	0.10	2
TDK1	Asp	9.467	0.781	0.113	0.007	2.215	4	23	179.71	2.83	0.06	5
SPK1	Asp	9.827	0.946	0.937	0.011	2.239	4	23	180.20	3.32	0.05	6
CPK1	Glu	3.561	2.655	1.660	0.012	2.435	4	23	181.19	4.31	0.03	16

Function refers to time-dependent rate kinetics (TDK), simple power-law kinetics (SPK), or constrained power-law kinetics (CPK) and 0 indicates that R_0 was assumed to be 0, whereas 1 indicates that R_0 was fit from the data; ln(a), ln(b), c, R_0, ln(d) are parameters of the various models; k is the number of model parameters; n is the number of fit data points; Bayes Information Criterion (BIC) is a measure of goodness of fit; ΔBIC is a fit relative to the best model; BIC weight (wBIC) is the contribution of the model to the best fit model; and model refers to the model numbers in the ESM 3 and 4

25 % >4 mm grains (Fig. 4). The homogeneity of this deposit is consistent with thorough mixing of the sediment, homogenous sediment supply, or minimally, mixing sufficient to homogenize any variation in sediment supply. Of note, the remains of a live-collected callianassid shrimp were found in the 1.05–1.10 m excavation layer indicating the presence of bioturbators capable of moving sediment through the entire excavated depth.

Sediment (^{210}Pb) age

Lead activity was measured from 11 of the same 1 cm thick layers used for the grain size analyses (Table 1). Lead analyses show declining $^{210}Pb_u$ activity below 0.15 m and reaching background levels by 0.50 m (Fig. 5). $^{210}Pb_u$ activities between 0 and 0.15 m do not decline, which suggests that the top 0.15 m of sediment is actively mixed on the decadal scale of ^{210}Pb decay; on the other hand, below this mixed layer, fine sediments preserve a chronologically ordered historical record which indicates that this sediment is not mixed on decadal scales.

The CIC age model assumes a constant initial ^{210}Pb concentration and a single net sediment accumulation rate. Based on the six analyzed layers between 0.15 and 0.41 m, the CIC age model estimated a sediment mass accumulation rate of 0.544 g cm^{-2} yr^{-1} ($r^2 = 0.941$). The CRS model assumes a constant rate of ^{210}Pb supply but allows the total sedimentation rate to vary. The CRS model estimates the sediment mass accumulation rate between each analyzed layer, and these values decreased down core ranging from 1.4 g cm^{-2} yr^{-1} in the 0–0.01 m layer to 0.2 g cm^{-2} yr^{-1} in the 0.30–0.31 and 0.35–0.36 m layers.

The two age models (CIC and CRS) yield largely consistent age estimates. Relative to the CRS model, the CIC model infers older ages near the top of the core and younger ages at depth. So, while all of the models converge on ages of ~65 yr for the 0.25–0.26 m layer, ~85 yr for the 0.30–0.31 m layer, and ~100 yr for the 0.35–0.36 m layer, there is greater disagreement at shallower layers (Table 1). The CRS age estimate for the 0.40–0.41 m layer is very uncertain due to the very low ^{210}Pb activity levels. Based on the ^{210}Pb data alone, there is little reason to favor one age model. One significant complication in reef sediment is carbonate chemistry and the various taphonomic processes that can result in carbonate loss and thus lead to post-depositional increases in lead concentration.

Shell (^{14}C/AAR) ages

The amino acid data had no notable outlier, and the correlation between Asp and Glu concentrations was highly significant with $r^2 > 0.98$. For the 11 jointly dated specimens, Asp and Glu D/L were highly correlated with calibrated carbon ages ($r^2 = 0.91$ and $r^2 = 0.93$, respectively). In fitting AAR calibration model, there was a noticeable bias associated with the choice of uncertainty distribution. Specifically, the calibration models fit using the gamma distribution to estimate uncertainty resulted in

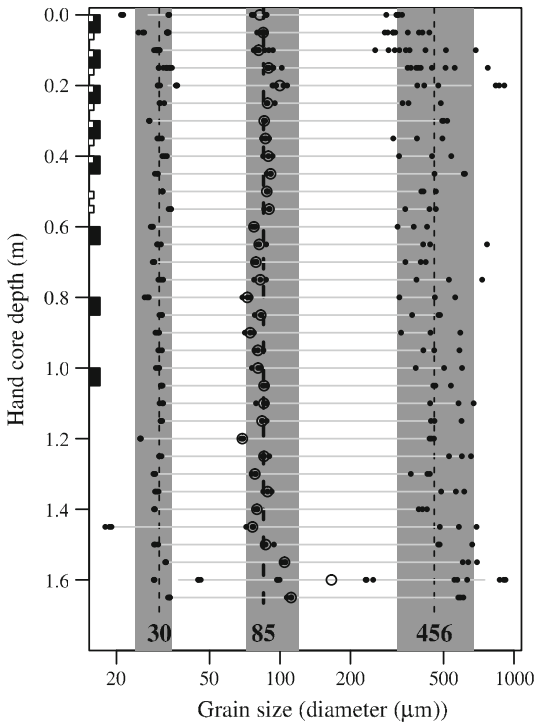

Fig. 3 Grain size analyses for the 80 mm diameter hand core every 5 cm down core. The *y*-axis indicates compacted core depth in meters. The *x*-axis indicates grain diameter on a log scale. *Black boxes* on the *left side* show the corresponding excavation layers from which shells were sampled for radiocarbon analyses, and *white boxes* on the *left side* indicate layers from which ^{210}Pb activity was measured. *Vertical dashed lines* indicate the 10th, 50th, and 90th grain size quantiles; the *gray boxes* indicate the 95 % confidence intervals on those quantiles; *black dots* represent individual measurements; and large *black circles* indicate median values of the replicate measurements

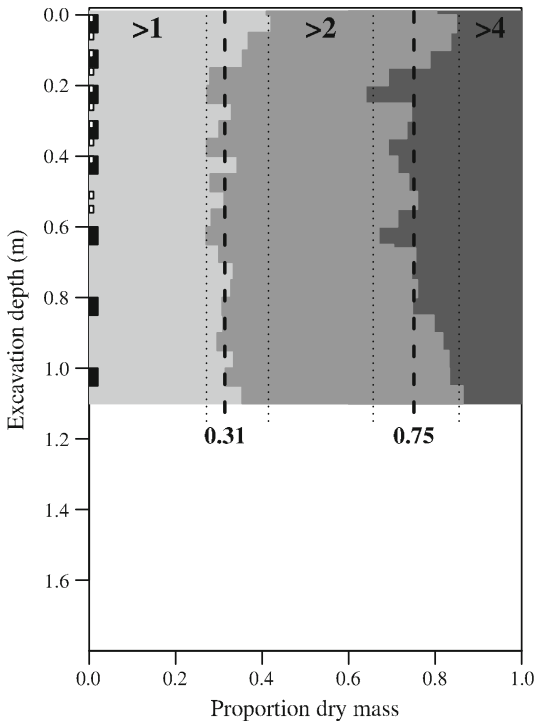

Fig. 4 Proportion of layer fraction dry weights from the 0.5 m × 0.5 m excavation retained by the >4 mm sieve (*dark gray*), >2 mm sieve (*medium gray*), and >1 mm sieve (*light gray*). *Black boxes* on the *left side* show the corresponding excavation layers from which shells were sampled for radiocarbon analyses, and *white boxes* on the *left side* indicate layers from which ^{210}Pb activity was measured. *Vertical thick dashed lines* indicate the median cumulative proportion in each fraction, and the thin dotted lines indicate the 95 % confidence intervals on those proportions

no shell with an inferred age <6 yrs, whereas using the lognormal distribution to estimate uncertainty resulted in nine shells with ages <6 yrs (ESM 3). The models fit using the lognormal distribution had much better fits (i.e., lower BIC scores) than those fit using the gamma distribution (Table 3). Nearly all of the Bayesian posterior distributions in ESM 4 show strong correlations between model parameters as seen by Allen et al. (2013). Some of the Bayesian posterior distributions show multiple modes indicating imperfect model fits (ESM 4), but the averaged age model contains only TDK and SPK functions indicating that these two models outperform CPK. The very low maximum Asp D/L and inferred age (0.25 and 625 yrs, respectively) make it unsurprising that CPK does not contribute to the final model. The very young age of these specimens and the imperfections in model fit results, both contribute to a relatively high median coefficient of variation of 1.7.

Inferred shell ages range from 1 to 625 yrs, and shell age increases with burial depth (Fig. 6). While the top ~0.15 m yields an essentially modern shell assemblage, every dated layer has an older median age than dated layers above although there is considerable overlap in the ages of individual shells (Fig. 6; Table 4). Individual shell ages and median shell age are both highly correlated with layer depth (Pearson's $r^2 = 0.92$ and $r^2 = 0.99$, respectively). These data indicate a sedimentary shell assemblage spanning the last 600 yrs that is preserved in stratigraphic order.

Discussion

Agreement between ^{210}Pb and ^{14}C/AAR chronologies

Despite different assumptions and sampled grain sizes, the ^{210}Pb and ^{14}C/AAR chronologies are remarkably consistent over the range of ages that can be directly compared (Fig. 7). While both ^{210}Pb age models are in general agreement with the ^{14}C/AAR chronology, the CIC age model yields a slope shallower than the unity line shown in

Table 4 Summary of excavation chronology by sampled layers

Sample		Shell ages (yr since 2012 AD)					Shell ages (yr relative to layer median)				
Interval (m)	*n*	2.275th	15.865th	Median	84.135th	97.725th	2.275th	15.865th	Median	84.135th	97.725th
0.00–0.05	6	2	3	4	57	167	−2	−2	0	53	163
0.10–0.15	11	2	3	8	19	22	−6	−5	0	11	14
0.20–0.25	10	7	22	55	133	188	−48	−33	0	78	133
0.30–0.35	12	11	52	88	187	356	−76	−36	0	100	268
0.40–0.45	6	114	132	152	198	199	−38	−20	0	46	47
0.60–0.65	11	132	195	258	298	364	−126	−63	0	40	106
0.80–0.85	12	281	319	429	506	607	−148	−110	0	77	178
1.00–1.05	12	406	463	535	573	610	−128	−71	0	38	76

Sample		Effective burial rate (mm yr^{-1})					Time-averaging (yr)	
Interval (m)	*n*	2.275th	15.865th	Median	84.135th	97.725th	Inner 68th	Inner 95th
0.00–0.05	6	0	0.6	6.2	10.1	12	55	165
0.10–0.15	11	−104	−5.5	6.9	30.9	160	15	21
0.20–0.25	10	−29	0.5	1.9	5.9	45	111	181
0.30–0.35	12	−9	−1.8	0.7	3.2	16	136	345
0.40–0.45	6	−11	−1.7	0.8	2.1	5	66	85
0.60–0.65	11	−10	0.9	1.7	3.4	24	104	232
0.80–0.85	12	−7	0.6	1.0	2.5	11	187	326
1.00–1.05	12	−24	−2.5	1.3	3.1	24	110	204

Sample interval in meters, number of dated shells, shell age quantiles, relative shell age quantiles, effective burial rate quantiles, and time-averaging calculated as the inner 68th quantile (84.135th age to 15.865th age) and inner 95th quantile (97.725th age to 2.275th age)

Fig. 7. The CRS age model more closely matches the ^{14}C/AAR chronology. In comparing the uncertainties plotted in Fig. 7, it is worth noting that the ^{210}Pb error plotted is a 1σ analytical error, and that the dated layer was 1 cm thick, whereas the ^{14}C/AAR time-averaging is the 1σ age range based on ~9 shells per 5 cm thick layer, thus including a greater sediment layer, time-averaging, and modelling uncertainties in addition to analytical error. Despite these sources of variation, the agreement between the ^{210}Pb and ^{14}C/AAR chronologies is exceptionally good. This suggests consistent sedimentary processes spanning the full range of sedimentary particle sizes.

Time-averaging and stratigraphic resolution

These data indicate a young shell assemblage in stratigraphic order. This is in stark contrast to the shell assemblages spanning similar burial depths from Rib and Bramble reefs that yielded age homogenous samples spanning the last ~3000 yr (Kosnik et al. 2007, 2009, 2013). Consistent with previous work, both ^{210}Pb and ^{14}C/AAR chronologies indicate that the top 0.15–0.2 m of sediment is actively mixed. The 0.20–0.25 m excavation layer yields a median shell age of 55 yrs (Table 4), and the ^{210}Pb analyses of the 0.20–0.21 m hand core layer yield an age of ~50 yrs (Table 1). Both of these lines of evidence could suggest that this sedimentary record might be capable of preserving fossil assemblages with ~50 yrs time-averaging.

A preferable approach to quantifying time-averaging is to determine the age of each shell relative to the layer's median shell age. By normalizing the data in this way, it is possible to examine changes in time-averaging down core independent of layer age (Fig. 8). In the samples from the top 0.15 m (combined 0–0.05 and 0.1–0.15 m layers), the 1σ age range is 19 yrs and the 2σ range is 125 yrs, whereas in samples below the top 0.2 m the median 1σ age range is 111 yrs and the 2σ age range is 218 yrs (Fig. 8). Despite a single exceptionally old specimen (oldest specimen was 186 yrs, whereas all other specimens were younger than 24 yrs) in the top layer, it is readily apparent that the degree of time-averaging increases dramatically below the top 0.2 m (Fig. 8). Time-averaging in surficial sediment is constrained by the impossibility of averaging future shells into the shallowest samples, but it is notable that above 0.6 m, relative age distributions appear to include more older shells than younger shells, whereas below 0.6 m, the relative age distributions appear more normally distributed (Fig. 8). These data support the general consensus that the age distribution of samples from surface collections are

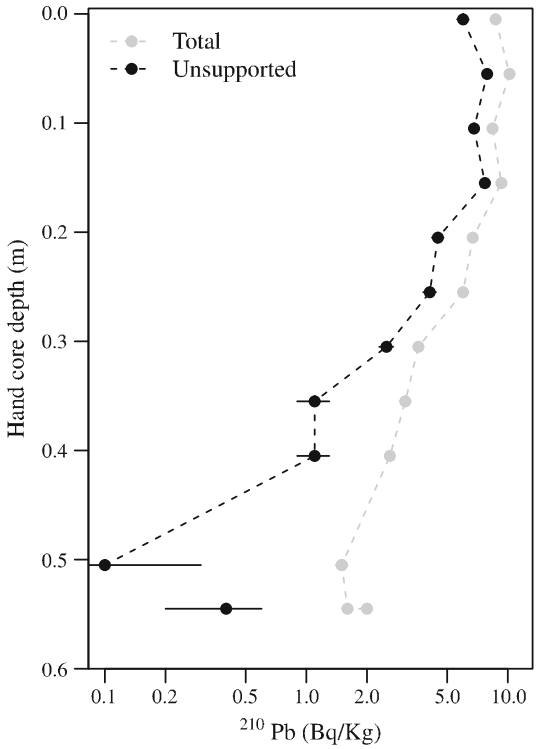

Fig. 5 Lead activity down core. The *x*-axis is lead activity on a log scale, and the *y*-axis is core depth in meters. Lead activity begins to decline from 0.15 m, and by 0.5 m, background levels are reached. The ^{210}Pb data are summarized in Table 1

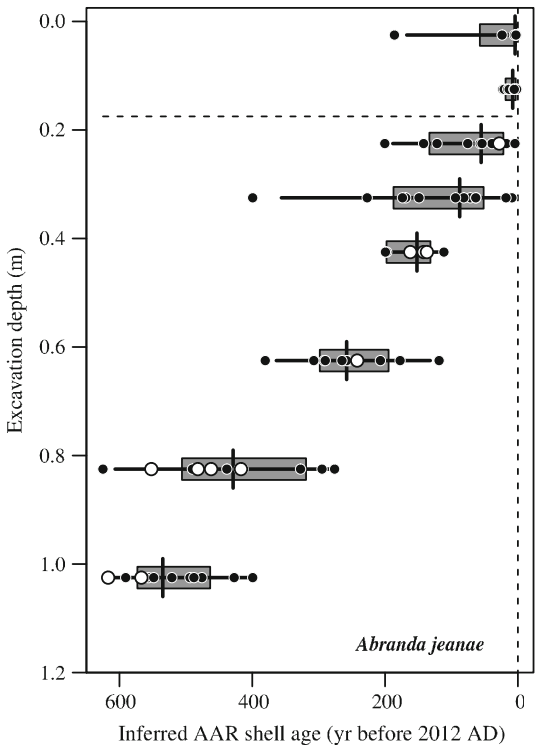

Fig. 6 Inferred shell ages with sediment depth. The *x*-axis is years before the year of collection (2012 AD), the *y*-axis is excavation depth in meters, *black dots* indicate the age of each AAR inferred shell age, *white dots* indicate the age of each ^{14}C dated shell, *horizontal lines* encompass 95 % of the data, the *horizontal bars* encompass 68 % of the data, and the *vertical bar* is the median layer age. The *dashed vertical line* is the year of collection (2012 AD). The ^{14}C/AAR data are summarized in Table 4

skewed (e.g., Kidwell 2013), and observations made in previous studies that the top 0.2 m of surficial sediment typically sampled by grab samplers do not reflect the properties of deeper sediments (Kosnik et al. 2007, 2009, 2013). Estimates of sedimentation or time-averaging derived from the surficial layer are indicative of internal depositional dynamics and not the aggrading sedimentary column. In these samples, the extent of time-averaging in shell assemblages buried below 0.2 m was 2–6× more than in surficial shell assemblages.

In this study and in previous studies by the same authors, subsurface samples shallower than 20 cm sample the same time interval as surface samples. In the context of detecting recent anthropogenic change, it is important to consider the dilution effect of this surficial layer and the related mixing. Time-averaging on the order of 19 to 125 yrs (1σ and 2σ, respectively) implies that a recent mass die-off will be mixed with the remains from normal annual mortality of $\sim$19 yrs. While time-averaging and bioturbation need to be quantified on a site specific basis, it is illustrative to examine the classic study of *Diadema* mass mortality (Greenstein 1989) in the context of what we now know about time-averaging in coral reef-associated sediment. Assuming a stable population size and an average life span of 4 yrs (Ogden and Carpenter 1987) implies a population turnover of 25 % per annum. Even a 100 % mass mortality event would yield only a mean mortality over the 1σ period of time-averaging of 29 %, or a 15.8 % more than background (18 yrs of 25 % and 1 yr of 100 %), and 3 yrs after the mass mortality event, the net increase is zero. That is a generous estimate as using the 2σ estimate of time-averaging yields an enrichment of only 2.4 %. These are, of course, only rough estimates as a precise estimate requires knowing the extent of time-averaging in the studied sediment, background mortality rates, and ideally, estimates of the rate of taphonomic loss of *Diadema* fragments within the sediment. Additionally, these calculations are based on the surface sediment, whereas deeper sediment layers have longer periods of time-averaging. In this case, however, the most likely effect of a mass mortality event such as the 1983 die-off may well be the lack of contribution in years after the mass mortality.

Sedimentation/shell burial rate

Both ^{210}Pb age models directly estimate sedimentation rate as mass flux that can be converted to depth using the

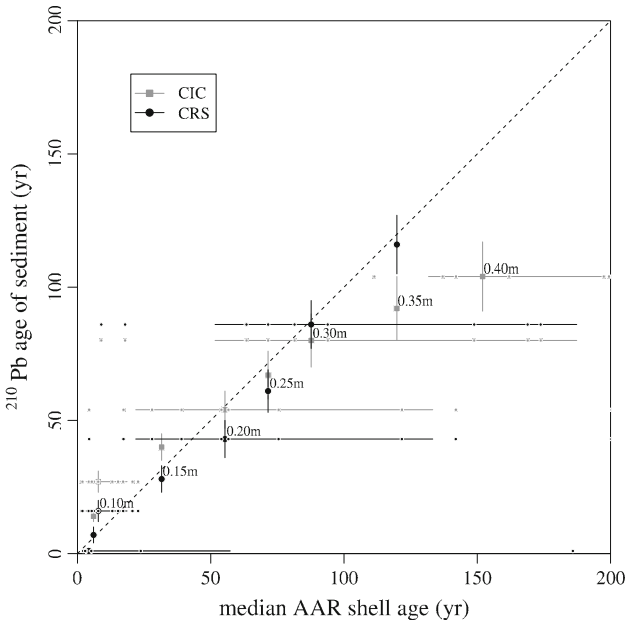

Fig. 7 Agreement between the ^{210}Pb chronology on the *y*-axis and the ^{14}C/AAR chronology on the *x*-axis. The *dashed 1:1 line* represents perfect agreement between the two age estimates. ^{210}Pb ages are single analyses with 1σ analytical error from a 1 cm layer, whereas ^{14}C/AAR ages are median shell age (*large circles*) and individual shell ages (*small dots*) from the 5 cm excavation layer with confidence intervals encompassing 68 % of the data based on the sample of dated shells from the layer (see Table 4). For sediment layers with ^{210}Pb ages but with no ^{14}C/AAR ages (e.g., layers 0.05, 0.15, 0.25, 0.35 m), the position on the *x*-axis is mean age of the adjacent dated shell layers. The CIC ^{210}Pb age model plotted in *gray* estimates a shallower slope than the *1:1 line* suggesting younger ages at depth than the CRS or ^{14}C/AAR ages. The CRS ^{210}Pb age model has very good agreement with ^{14}C/AAR age estimates. As expected, neither ^{210}Pb age model works well in the top 0.15 m of sediment. The ^{210}Pb data are summarized in Table 1 and the ^{14}C/AAR data are summarized in Table 4

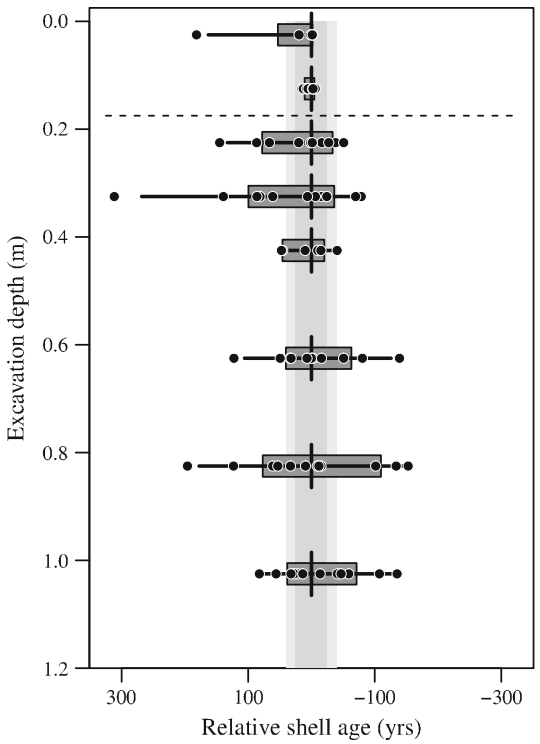

Fig. 8 Relative shell age with sediment depth. The *x*-axis is shell age in years relative to the layer's median age, the *y*-axis is excavation depth in meters, individual *black dots* represent the relative age of each shell, *horizontal lines* encompassing 95 % of the data, the *horizontal bars* encompass 68 % of the data, and the *vertical bar* is the median layer age (see Table 4). The *light gray vertical box* approximates the time accounted for by the 5 cm collection interval

measured sediment density (Table 1). While the CIC model estimates a constant sedimentation accumulation rate of 3.9 mm yr^{-1} [(0.544 g cm^{-2} yr^{-1} / 1.4 g cm^{-3}) × 10 mm cm^{-1}], the CRS model allows the mass accumulation rate to vary. The CRS model sediment accumulation rates decline down core, especially through the top 0.15 m. The CRS model estimates a sedimentation rate of 9.0 mm yr^{-1} for the surface (0.00–0.01 m) layer, declining to a rate of ~1.6 mm yr^{-1} in the two layers below 0.3 m. Breaking the CRS sedimentation rates into the upper mixed layer and the deeper layers showing clear decline in ^{210}Pb activity (see Fig. 5) yields average sedimentation rates of 6.0 and 2.2 mm yr^{-1} for 0–0.16 m and 0.2–0.36 m, respectively.

The shell ages can be used to calculate effective shell burial rate in several different ways. A simple linear regression of age and burial depth yields a highly significant relation ($r^2 = 0.84$) and a burial rate of 1.6 mm yr^{-1}. This is analogous to the single sedimentation rate provided by the ^{210}Pb CIC model, although the shell burial rate is half the ^{210}Pb CIC sedimentation rate. The intercept of this regression is also significant and suggests that accumulation starts at 0.145 m. Fitting the shells collected from layers deeper than 0.2 m separately yields a burial rate of 1.4 mm yr^{-1} ($r^2 = 0.81$), a value half of that estimated by the CIC model.

Alternatively, one can examine the difference in shell age between sequential layers. This estimate uses the difference between the two layers as the depth of sediment and all pairwise differences in shell ages between adjacent layers. This results in a distribution of burial rates for each depth (Fig. 9; Table 4). These results are most comparable to the CRS sedimentation rates and indicate a clear change shell burial rate between 0.15 and 0.2 m depth. Interpretation of the shell burial rates in the top 0.15 m is complicated by the certainty that these shells are still being actively mixed, and the likelihood that the total sediment volume is being still being reduced by taphonomic processes. In the top 0.15 m, the shell burial rate averages 5.6 mm yr^{-1}. Deeper than 0.2 m, the shell burial rate ranges between 0.7 and 1.9 mm yr^{-1} with a mean burial

rate of 1.2 mm yr^{-1} (Table 4). In comparison, CRS sedimentation rates are 6.0 and 2.2 mm yr^{-1} for the same depth ranges. Given the uncertainties and biases of the two different analyses, these two values are remarkably similar.

Both datasets indicate higher sedimentation/burial rates in the surficial layer, but the magnitude of this difference is a factor of $\sim$2 (lead sedimentation rates are 2.7$\times$ higher, whereas shell burial rates are 4.6$\times$ higher). It is likely that all the sedimentation rates from the top layer are inflated relative to deeper layers due to surface sediments being less compacted and/or taphonomically less altered. Relative to research at other locations on the GBR, the OTR lagoon has little evidence of size-selective sedimentary processes at work.

In the early 1980s, Davies Reef lagoon was the subject of numerous sedimentological and bioturbation studies (e.g., Tudhope and Scoffin 1984; Tudhope and Risk 1985; Tudhope 1989). Based on four dates, Tudhope (1989) estimated the sedimentation rate to be 3.4 mm yr^{-1} over the past 640 yrs, 1.4 mm yr^{-1} between 640 and 2,400 yrs. The estimate of the last 640 yrs is based on a *Callista* valve aged 642 yrs sampled at 2.5 m (including a −0.3 m depth correction for estimated living depth = 3.4 mm yr^{-1} over the past 640 yrs), and bulk carbon ages of sediment collected from 1 m minus the bulk age of surface sediment and accounting for the surface mixed layer ("a few tens of centimeters/100 years" p. 1044). The estimate for the sedimentation rate between 640 and 2,400 yrs is based on a bulk carbon age collected from 4.75 m aged 3,672 yrs (1.3 mm yr^{-1}), but subtracting the estimated time required to transport the sediment to the site (1,200–1,400 yrs) yields estimates of 1.9–2.1 mm yr^{-1}. Despite the limited number of dates, these sedimentation rates are similar to those calculated here.

Dates determined during geochronologic and taphonomic studies of Rib and Bramble Reef can also be used to estimate sedimentation rates. The excavation sites at Rib and Bramble reefs are sedimentary environments very similar to Davies Reef. In the Rib Reef lagoon, the median age of *Pinguitellina robusta* sampled between 0.3 and 1.1 m was 636 yrs = 1.7 mm yr^{-1} (Kosnik et al. 2013). In the Bramble Reef lagoon, the median age of *Pinguitellina* sampled in the top 1.25 m was 516 yrs = 2.4 mm yr^{-1} (Kosnik et al. 2013). As the Rib and Bramble Reef cores are also largely time homogenous, it would be possible to decrease these rates by $\sim$3$\times$ by sampling similarly aged shells at $\sim$0.3 m. Additional taxa with different inherent durability were dated from the same Rib and Bramble Reef cores (Kosnik et al. 2009); sedimentation rates calculated for each taxon differ even for the same core layer. Despite that, the shell burial rates are similar to that seen in the OTR lagoon data.

One explanation for a decline in shell burial rate is increased sediment compaction associated with decreased sediment water content with depth. This would be consistent with the increasing difficulty of collecting deeper excavation layers in the field, but not consistent with the measured sediment bulk densities (Table 1). The top 0.2 m was easily penetrated and quickly collected, but sediment deeper than $\sim$0.6 m was notably more difficult to penetrate and required more time to collect. If dewatering was the sole reason for a decline in burial rate with depth, then the amount of time recorded per 5 cm layer should also increase with depth. However, there is no correlation between layer median burial rate and the degree of time-averaging in layers below 0.2 m [Pearson's $p \geq 0.69$ (0.83 for 1σ age range, 0.69 for 2σ age range)]. While we have insufficient data to definitively test the dewatering hypothesis, we find no support for it.

The surface layer is actively mixed by a variety of physical and biological processes. The exceptionally fine grain size distribution suggests that reworking by wave energy is quite rare, but collections from the surface sediment yielded large numbers of living mollusks, arthropods, and annelids suggesting significant bioturbation. Size-specific sorting has been documented in reef

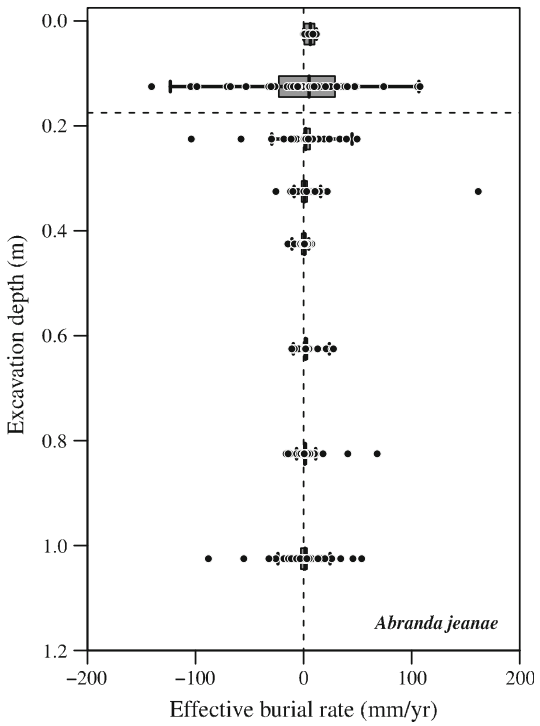

Fig. 9 Effective shell burial rate. The *x*-axis is effective burial rate between sequential layers in mm yr^{-1}, the *y*-axis is excavation depth in meters, *black circles* represent the pairwise comparisons between each shell in the layer to each shell in the layer above, *horizontal lines* encompass 95 % of the data, and the *horizontal bars* encompass 68 % of the data (see Table 4). The *vertical dashed line* is an effective sedimentation rate of 0 mm yr^{-1}. All layers have a positive effective sedimentation rate (see Table 4)

sediments (e.g., Tudhope and Scoffin 1984), and this is anecdotally supported by a slightly smaller >4 mm fraction in the surface layers than in the rest of the excavation (Fig. 4) in conjunction with the observation that much of the larger material in the surface 0.1 m was alive at the time of collection (e.g., 56 % of *Abranda* sampled from the 0 to 0.05 m layer were alive). However, bioturbation is insufficient to obscure stratigraphic order in this sediment. The most promising hypothesis to explain the observed decrease in sedimentation rate is the loss of sediment through taphonomic processes.

Sediment taphonomy

Carbonate sediment is chemically active and an important part of the global carbon cycle. While the dissolution of carbonate grains under natural conditions is incredibly complex, laboratory experiments have shown that grain microstructure and size can each influence rates of reaction by a factor of 7 at the same saturation state (Walter and Morse 1984). Very high rates of fine sediment loss can be used to explain fine surface layers over coarse deeper sediments such as those documented by Tudhope and Scoffin (1984) and Kosnik et al. (2007, 2009, 2013), but the One Tree lagoon data presented here lack significant down core changes in the complete grain size distributions (Figs. 3, 4). This means that changes in sedimentation rate cannot be driven by preferential loss of a particular size fraction, at least any preferential loss of grains within the dominant <1 mm size fraction.

Another potential explanation for the decline in burial/sedimentation rates with depth is continued taphonomic loss of sediment at depth. If we assume that the two deepest excavation layers are below the taphonomically active zone, then the final shell burial rate is 1.2 mm yr^{-1}. Assuming 1.2 mm yr^{-1} is the net rate, sediment from the top 0.2 m would have a 21 % chance of survival, sediment from 0.2–0.25 m and 0.3–0.35 m layers would have 93 % chance of survival, and sediment from 0.4–0.45 m and 0.6–0.65 m layers would have 95 % chance of survival. Given the uncertainties in these estimates, it is reasonable to suggest that layers deeper than 0.2 m are within depth of final burial, but that the probability of sediment above 0.2 m, i.e., the taphonomically active zone, being buried below 0.2 m, i.e., the depth of final burial, is ~21 % (sensu Olszewski 2004). This explanation does not preclude changes in time-averaging with depth, especially if per grain sediment preservation rates vary. The time-averaging data are consistent with the condensation implied by a 15 % survival rate of non-mollusk shell sediment (although these data are not independent from the burial depth data above). The 1σ time-averaging below 0.2 m is 111 versus 19 yrs above 0.2 m, indicating deeper deposits can be derived by these surface sediments with 16 % survival of non-mollusk remains.

Another indication of surficial sediment loss is that the surface sample (0.0–0.01 m) had lower ^{210}Pb activity than the other three mixed layers. This suggests that the key assumption of the CIC model is not true in this sediment. The observed increase in ^{210}Pb activity between the surface layer and the 0.05–0.06 m layer is consistent with a 16 % loss of carbonate from the surface layer. A 16 % loss is consistent with the 18–30 % loss estimated in experimental studies of microborers in the Davies Reef lagoon (Tudhope and Risk 1985); as this 16 % estimate is conservative in that, it assumes no taphonomic loss from the 0.05 to 0.06 m layer.

The lead sediment accumulation rate data can also be used to estimate the loss of sediment through digenetic processes. Assuming that the minimum sediment accumulation rate represents the final net sedimentation rate, it is possible to calculate the amount of sediment that must be lost from each layer to reach the minimum sedimentation rate. This approach estimates sediment survival in the top layer (0–0.01 m) at 16 %, and preservation rate has a strong linear relation ($r^2 = 0.92$) with depth, increasing at 0.25 % per mm core depth. This estimate of sediment preservation probability is consistent and entirely independent of the 21–16 % estimate derived from the shell data.

Implications

While the top 0.2 m is actively mixed, the top meter of lagoonal sediment preserves a stratigraphically ordered deposit spanning the last 600 yrs. Despite different assumptions, ^{210}Pb and ^{14}C/AAR chronologies are remarkably similar indicating consistency in sedimentary processes across sediment grain sizes spanning more than three orders of magnitude (0.1–10 mm). Both ^{210}Pb and ^{14}C/AAR data suggest that only ~16 % surface sediment in the OTR lagoon will be buried, whereas ~84 % of the surface sediment with be recycled through the system. ^{210}Pb ages inferred using the CRS model show the highest level of agreement with ^{14}C/AAR age estimates. Molluscan time-averaging in this sediment is ~110 yrs per 5 cm layer. While not a high-resolution record, at least some reef-associated sediment is suitable for paleoecological studies spanning the period of Western colonization and development. This sedimentary deposit, and others like it, should be useful, albeit not ideal, for quantifying anthropogenic impacts on coral reef systems.

Acknowledgments The author list is alphabetical following the lead author, and each coauthor contributed time, thought, and effort to this paper. We thank: E. Connolly, P. Hallam, J. Martinelli, P.

McCracken, and M. Philips for assistance collecting samples; J. Reiffel and R. Graham for logistical assistance and hospitality at One Tree Island Research Station; S. Duce for the Mastersizer analyses; H. Bell for the excavation sediment weights; K. Cooper for the AAR analyses, and J. Goralewski for the ^{210}Pb labwork; and K. Wilson and two anonymous reviewers for comments on the manuscript. Funding: Australian Research Council Future Fellowship FT0990983 (Fieldwork and MAK support); Australian Institute of Nuclear Science and Engineering Awards #12/093 and #13/528 (^{210}Pb and ^{14}C analyses); and US National Science Foundation grant EAR-09-9415 (AAR analyses). Open access made possible in part by a contribution by the Department of Biological Sciences, Macquarie University.

Open Access This article is distributed under the terms of the Creative Commons Attribution License which permits any use, distribution, and reproduction in any medium, provided the original author(s) and the source are credited.

References

Allen AP, Kosnik MA, Kaufman DS (2013) Characterizing the dynamics of amino acid racemization using time-dependent reaction kinetics: A Bayesian approach to fitting age-calibration models. Quat Geochronol 18:63–77

Appleby PG (2001) Chronostratigraphic techniques in recent sediments. In: Last WM, Smol JP (eds) Tracking environmental change using lake sediments, vol 1., Basin analysis, coring and chronological techniques. Kluwer Academic Publishers, Dordrecht, pp 171–203

Appleby PG, Oldfield F (1978) The calculation of lead-210 dates assuming a constant rate of supply of unsupported ^{210}Pb to the sediment. Catena 5:1–8

Bronk Ramsey C (2009) Bayesian analysis of radiocarbon dates. Radiocarbon 51:337–360

Cummins H, Powell EN, Stanton RJ, Staff G (1986) The rate of taphonomic loss in modern benthic habitats: how much of the potentially preservable community is preserved? Palaeogeogr Palaeoclimatol Palaeoecol 52:291–320

Druffel ERM, Griffin S (2004) Southern Great Barrier Reef Coral Radiocarbon Data. IGBP PAGES/World Data Center for Paleoclimatology, Data Contribution Series #2004-093, NOAA/NCDC Paleoclimatology Program, Boulder CO, USA.

Fink D, Hotchkis M, Hua Q, Jacobsen G, Smith AM, Zoppi U, Child D, Mifsud C, van der Gaast H, Williams A, Williams M (2004) The ANTARES AMS Facility at ANSTO. Nuclear Instruments and Methods in Physics Research B 223–224:109–115

Fabricius KE, Fabricius FH (1992) Re-assessment of ossicle frequency patterns in sediment cores: rate of sedimentation related to *Acanthaster planci*. Coral Reefs 11:109–114

Flessa KW, Cutler AH, Meldahl KH (1993) Time and taphonomy: Quantitative estimates of time averaging and stratigraphic disorder in a shallow marine habitat. Paleobiology 19:266–286

Greenstein BJ (1989) Mass mortality of the West-Indian echinoid *Diadema antillarum* (Echinoidermata: Echinoidea): A natural experiment in taphonomy. Palaios 4:487–492

Goldberg ED (1963) Geochronology with ^{210}Pb. Radioactive dating. International Atomic Energy Agency, Vienna, pp 121–131

Hollins EH, Harrison JJ, Jones BJ, Zawadzki A, Heijnis H, Hankin S (2011) Reconstructing recent sedimentation in two urbanised coastal lagoons (NSW, Australia) using radioisotopes and geochemistry. J Paleolimnol 46:579–596

Hua Q, Jacobsen GE, Zoppi U, Lawson EM, Williams AA, McGann MJ (2001) Progress in radiocarbon target preparation at the ANTARES AMS centre. Radiocarbon 43:275–282

Kaufman DS, Manley WF (1998) A new procedure for determining DL amino acid ratios in fossils using reverse phase liquid chromatography. Quat Sci Rev 17:987–1000

Keesing JK, Bradbury RH, DeVantier LM, Riddle MJ, De'ath G (1992) Geological evidence for recurring outbreaks of the crown-of-thorns starfish: A reassessment from an ecological perspective. Coral Reefs 11:79–85

Kidwell SM (2013) Time-averaging and fidelity of modern death assemblages: building a taphonomic foundation for conservation palaeobiology. Palaeontology 56:487–522

Kidwell SM, Best MMR, Kaufman DS (2005) Taphonomic trade-offs in tropical marine death assemblages: Differential time averaging, shell loss, and probable bias in siliciclastic vs. carbonate facies. Geology 33:729–732

Kosnik MA, Kaufman DS (2008) Identifying outliers and assessing the accuracy of amino acid racemization measurements for geochronology: II. Data screening. Quat Geochronol 3:328–341

Kosnik MA, Kaufman DS, Hua Q (2008) Identifying outliers and assessing the accuracy of amino acid racemization measurements for use in geochronology: I. Age calibration curves. Quat Geochronol 3:308–327

Kosnik MA, Kaufman DS, Hua Q (2013) Radiocarbon-calibrated multiple amino acid geochronology of Holocene molluscs from Bramble and Rib Reefs (Great Barrier Reef, Australia). Quat Geochronol 16:73–86

Kosnik MA, Hua Q, Kaufman DS, Wüst RA (2009) Taphonomic bias and time-averaging in tropical molluscan death assemblages: Differential shell half-lives in Great Barrier Reef sediment. Paleobiology 34:565–586

Kosnik MA, Hua Q, Jacobsen GE, Kaufman DS, Wüst RA (2007) Sediment mixing and stratigraphic disorder revealed by the age-structure of *Tellina* shells in Great Barrier Reef sediment. Geology 35:811–814

Kowalewski M (1996) Time-averaging, overcompleteness, and the fossil record. J Geol 104:317–326

Krause RA, Barbour SL, Kowalewski M, Kaufman DS, Romanek CS, Simões MG, Wehmiller JF (2010) Quantitative comparisons and models of time-averaging in bivalve and brachiopod shell accumulations. Paleobiology 36:28–452

Meldahl KH, Flessa KW, Cutler AH (1997) Time-averaging and postmortem skeletal survival in benthic fossil assemblages: quantitative comparisons among Holocene environments. Paleobiology 23:207–229

Ogden JC, Carpenter RC (1987) Species profiles: life histories and environmental requirements of coastal fishes and invertebrates (south Florida) – long-spined black sea urchin. U.S. Fish and Wildlife Service Biological Report 82(11.77). U.S. Army Corps of Engineers TR EL-82-4, pp 1–17

Oldfield F, Appleby PG (1984) Emperical testing of ^{210}Pb-dating models for lake sediments. In: Haworth EY, Lund JWG (eds) Lake sediments and environmental history. University of Minnesota Press, Minneapolis, pp 93–124

Olszewski TD (2004) Modeling the influence of taphonomic destruction, reworking, and burial on time-averaging in fossil accumulations. Palaios 19:39–50

Pandolfi JM (1992) A palaeobiological examination of the geological evidence for recurring outbreaks of the crown-of-thorns starfish, *Acanthaster planci* (L.). Coral Reefs 11:87–93

R Development Core Team (2013) R: A language and environment for statistical computing: Vienna, Austria, R Foundation for Statistical Computing, http://www.R-project.org

Reimer PJ, Baillie MGL, Bard E, Bayliss A, Beck JW, Blackwell PG, Bronk Ramsey C, Buck CE, Burr GS, Edwards RL, Friedrich M, Grootes PM, Guilderson TP, Hajdas I, Heaton TJ, Hogg AG, Hughen KA, Kaiser KF, Kromer B, McCormac FG, Manning SW, Reimer RW, Richards DA, Southon JR, Talamo S, Turney

CSM, van der Plicht J, Weyhenmeyer CE (2009) IntCal09 and Marine09 radiocarbon age calibration curves, 0–50,000 years - cal BP. Radiocarbon 51:1111–1150

Tudhope AW (1989) Shallowing upwards sedimentation in a coral reef lagoon, Great Barrier Reef of Australia. J Sediment Petrol 59:1036–1051

Tudhope AW, Scoffin TP (1984) The effects of *Callianassa* bioturbation on the preservation of carbonate grains in Davies reef lagoon, Great Barrier Reef, Australia. J Sediment Petrol 54:1091–1096

Tudhope AW, Risk MJ (1985) The rate of dissolution of carbonate sediments by microboring organisms, Davies reef, Australia. J Sediment Petrol 55:440–447

Walbran PW, Henderson RA, Faithful JW, Polach HA, Sparks RJ, Wallace G, Lowe DC (1989) Crown-of-thorns starfish outbreaks on the Great Barrier Reef: a geological perspective based upon the sediment record. Coral Reefs 8:67–78

Walter LM, Morse JW (1984) Total versus reactive surface areas of skeletal carbonates during carbonate dissolution: Effect of grain size. J Sediment Petrol 54:1081–1090

Wehmiller JF, Miller GH (2000) Aminostratigraphic dating methods in Quaternary geology. In: Noller JS, Sowers JM, Lettis WR (eds) Quaternary geochronology: methods and applications. American Geophysical Union, Washington DC, pp 187–222